Experimental Section

Synthesis of FeS_2/RGO

FeS_2/RGO was prepared by a hydrothermal method. In brief, 10 mg of GO was dispersed in 50 mL of deionized water under ultrasonic dispersion for 1 h, to which 1.5 mL of ammonium hydroxide, 1.0 mmol of ferric nitrate, 2.0 mmol of thioacetamide were co-added under magnetic stirring to form a homogeneous solution. The mixed suspension was transferred to a Teflon-lined autoclave and kept at 160 ℃ for 24 h. The products were collected and then washed with deionized water and alcohol several times, and then dried at 60 ℃ under vacuum to obtain FeS_2/RGO. For comparison, RGO was prepared by the same procedure without addition of ammonium hydroxide, ferric nitrate and thioacetamide.

Electrochemical experiments

Electrochemical measurement was performed on a CHI-660E electrochemical workstation. FeS_2/RGO coated on carbon cloth (1×1 cm^2, 0.5 mg cm^{-2}), Hg/HgO and platinum foil were used as working, reference and counter electrodes, respectively. All potentials reported in this work were referenced to reversible hydrogen electrode (RHE) scale by $E_{RHE} = E_{Hg/HgO} + (0.098 + 0.0591 \times pH)$[1, 2]. The NO_3RR measurements were carried out in Ar-saturated 0.5 M Na_2SO_4 (pH=6.8) + 0.1 M $NaNO_3$ (pH=6.6) electrolyte using an H-type two-compartment electrochemical cell separated by a Nafion 211 membrane. The Nafion membrane was pretreated by heating it in 5% H_2O_2 aqueous solution at 80 °C for 1 h and then in deionized water at 80 °C for another 1 h. After each chronoamperometry test for 1 h, the remaining NO_3^-, the produced NH_3 and other possible by-products (NO_2^- and N_2H_4) were analyzed by various colorimetric methods using UV-vis absorbance spectrophotometer (MAPADA P5), while the gas products (H_2, N_2) were analyzed by gas chromatography (Shimadzu GC2010).

Determination of NH_3

NH_3 in electrolyte was quantitatively determined by the indophenol blue method[3]. Coloring solution was prepared by mixing 2 mL NaOH solution (1 M), 5 % salicylic

acid and 5 % potassium sodium tartrate. 1 mL NaClO (0.05 M) and $C_5FeN_6Na_2O$ (0.2 mL, 1wt.%). Then, the coloring solution was added to 2 mL diluted electrolyte. After the incubation for 2 h at room temperature, the mixed solution was subjected to UV-vis measurement using the absorbance at 655 nm wavelength. The concentration-absorbance curves were calibrated by the standard NH_4Cl solution with a series of concentrations, and the NH_3 yield rate and Faradaic efficiency (FE) were calculated by the following equation[4-7]:

$$NH_3 \text{ yield } (\mu g \text{ h}^{-1} \text{ mg}_{cat.}^{-1}) = \frac{c_{NH_3} \times V}{t \times A} \quad (1)$$

Faradaic efficiency was calculated by the following equation:

$$\text{Faradaic efficiency } (\%) = \frac{8 \times F \times c_{NH_3} \times V}{17 \times Q} \times 100\% \quad (2)$$

where c_{NH3} (μg mL^{-1}) is the measured NH_3 concentration, V (mL) is the volume of the electrolyte, t (h) is the reduction time, A (cm^{-2}) is the surface area of CC (1×1 cm^2) , F (96500 C mol^{-1}) is the Faraday constant, 17 represents the molar mass of NH_3, Q (C) is the quantity of applied electricity.

Determination of NO_2^-

NO_2^- in electrolyte was quantitatively determined by a Griess test[8]. Coloring solution was prepared by adding 0.1 g N-(1-naphthyl)-ethylenediamine hydrochloride, 1.0 g sulfonamide and 2.94 mL H_3PO_4 in 50 m L deionized water. Then, 0.2 mL coloring solution was added to 2 mL diluted electrolyte. After the incubation for 20 min at room temperature, the mixed solution was subjected to UV-vis measurement using the absorbance at 540 nm wavelength. The concentration-absorbance curves were calibrated by the standard KNO_2 solution with a series of concentrations.

Determination of NO_3^-

NO_3^- in electrolyte was quantitatively determined by a reported method[9]. The electrolyte was collected and diluted to the detection range. 2 mL diluted electrolyte was mixed with 40 μL 1 M HCl containing 4.0 μl 0.8 wt% sulfamic acid. After the incubation for 20 min at room temperature, the mixed solution was subjected to UV-vis measurement using the absorbance at 220 nm wavelength. The concentration-

absorbance curves were calibrated by the standard KNO_3 solution with a series of concentrations.

Determination of N_2H_4

N_2H_4 in electrolyte was quantitatively determined by a Watt and Chrisp method[10]. Coloring solution was prepared by mixing 300 mL C_2H_5OH, 5.99 g $C_9H_{11}NO$ and 30 mL HCl. Then, 5 mL color solution was added into 5 mL electrolyte. After the incubation for 20 min at room temperature, the mixed solution was subjected to UV-vis measurement using the absorbance at 455 nm wavelength. The concentration-absorbance curves were calibrated by the standard N_2H_4 solution with a series of concentrations.

Characterizations

The X-ray diffraction pattern was measured on Rigaku D/max 2400 diffractometer. Scanning electron microscopy (SEM) was collected on a JSM-6701 microscope. Transmission electron microscopy (TEM) and high-resolution transmission electron microscopy (HRTEM) images were carried out on a Tecnai G2 F20 microscope. X-ray photoelectron spectroscopy (XPS) analysis was performed on a PHI 5702 spectrometer. The absorbance was measured by MAPADA ULM 1912006 UV-Vis spectrophotometer. The ^1H nuclear magnetic resonance (NMR) test was performed on a 500 MHz Bruker superconducting magnetic spectrometer.

Calculation details

Spin-polarized DFT calculations were carried out using a Cambridge sequential total energy package (CASTEP). The Perdew–Burke–Ernzerhof (PBE) generalized gradient approximation (GGA) functional was used to model the exchange-correlation interactions. The DFT-D correction method was used to describe the van der Waals interactions throughout the calculations. The electron wave functions were expanded using plane waves with a cutoff energy of 500 eV. The convergence tolerance was set to be 1.0×10^{-5} eV for energy and 0.1 eV $Å^{-1}$ for force. The Brillouin zone was sampled by 3×3×1 Monkhorst−Pack k-point mesh. The FeS_2 (200) was modeled and a vacuum region of 15 Å was used to separate adjacent slabs. The adsorption energy (ΔE) is calculated as[11]

$$\Delta E = E_{ads/slab} - E_{ads} - E_{slab} \quad (3)$$

where $E_{ads/slab}$, E_{ads} and E_{slab} are the total energies for adsorbed species on slab, adsorbed species and isolated slab, respectively.

The computational hydrogen electrode (CHE) model was adopted to calculate the Gibbs free energy change (ΔG) for each elementary step as follows:

$$\Delta G = \Delta E + \Delta ZPE - T\Delta S \quad (4)$$

where ΔE is the adsorption energy, ΔZPE is the zero-point energy difference and $T\Delta S$ is the entropy difference between the gas phase and adsorbed state. The entropies of free gases were acquired from the NIST database. Given that it is difficult to directly calculate the energy of charged NO_3^-, the adsorption free energy of NO_3^- ($\Delta G(*NO_3)$) was calculated with assistance of the gaseous HNO_3 as follows[12]

$$\Delta G(*NO_3) = G(*NO_3) - G(*) - [G(HNO_3) - 0.5 \times G(H_2)] + \Delta G_{correct} \quad (5)$$

where $G(*)$ and $G(*NO_3)$ are the Gibbs free energies of the bare catalyst and that with the adsorbed NO_3^-, respectively. $G(HNO_3)$ and $G(H_2)$ represent the Gibbs free energies of HNO_3 and H_2 molecule, respectively.

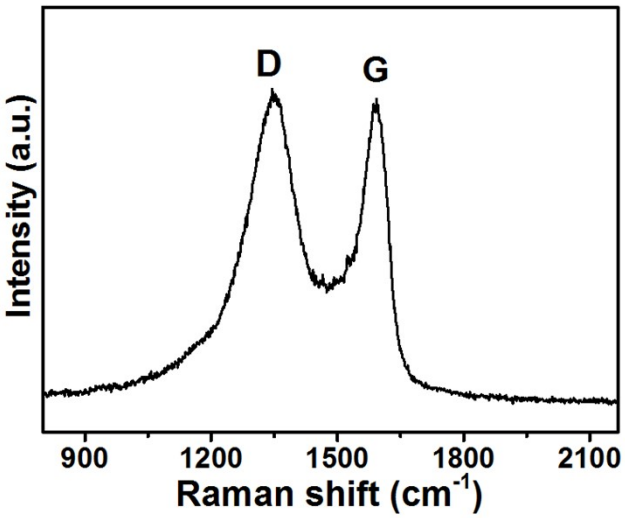

Fig. S1. Raman spectra of FeS_2/RGO

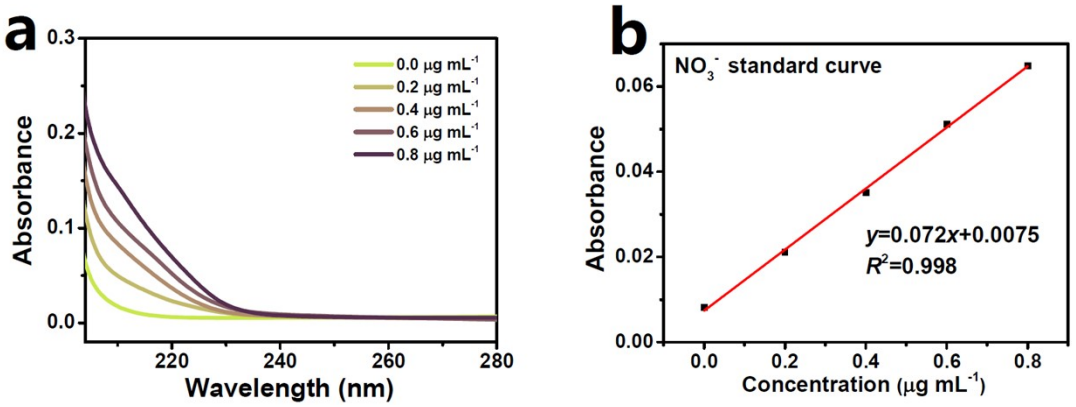

Fig. S2. (a) UV-vis absorption spectra of NO_3^- assays after incubated for 20 min at ambient conditions. (b) Calibration curve used for calculation of NO_3^- concentrations.

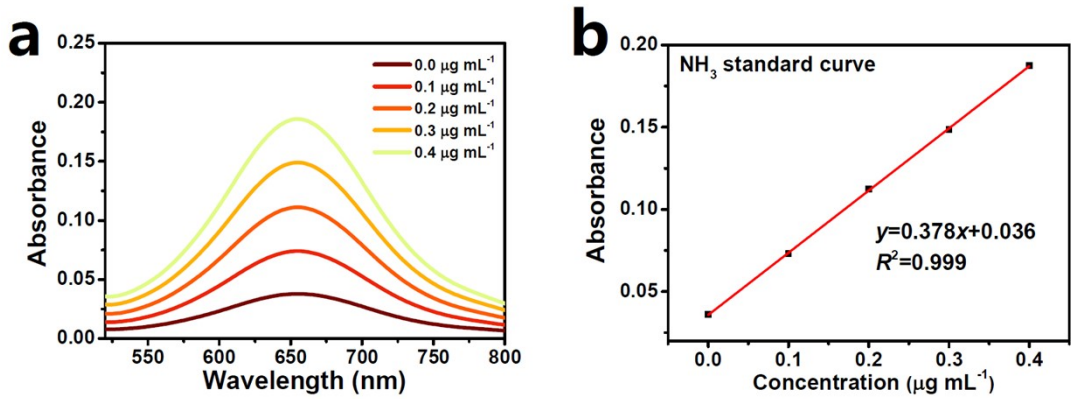

Fig. S3. (a) UV-vis absorption spectra of NH_4^+ assays after incubated for 2 h at ambient conditions. (b) Calibration curve used for the calculation of NH_3 concentrations.

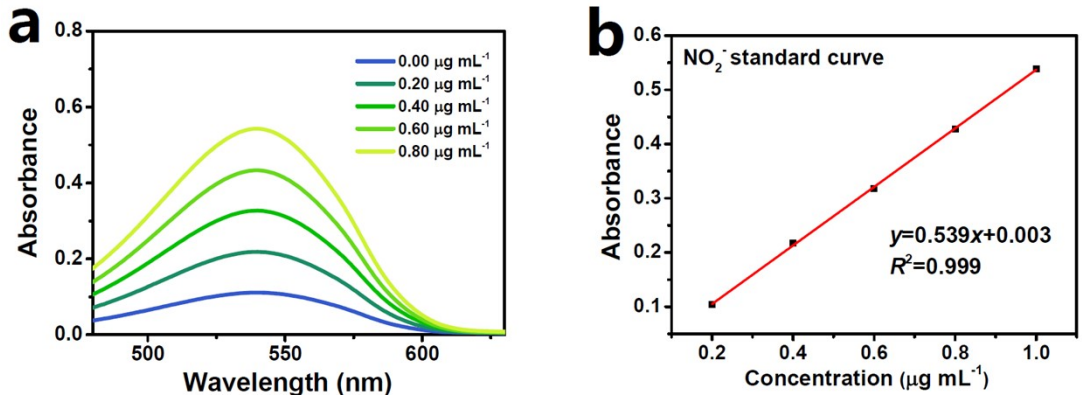

Fig. S4. (a) UV-vis absorption spectra of NO_2^- assays after incubated for 20 min at ambient conditions. (b) Calibration curve used for calculation of NO_2^- concentrations.

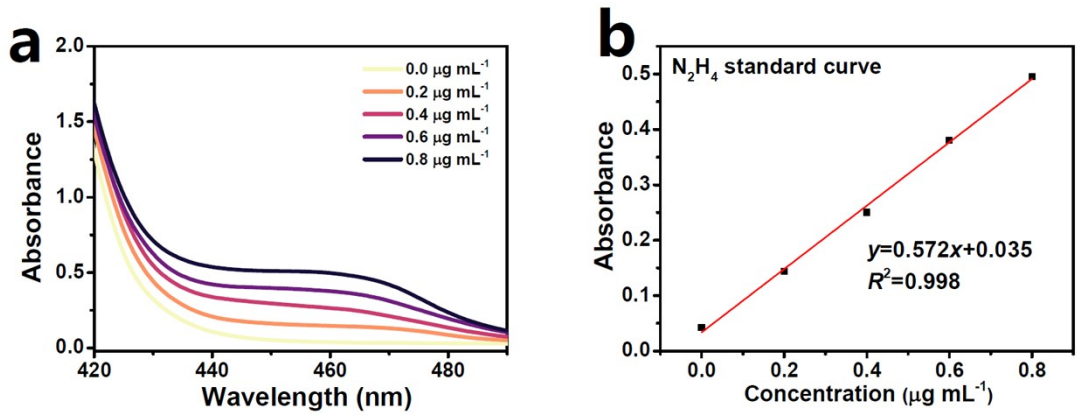

Fig. S5. (a) UV-vis absorption spectra of N_2H_4 assays after incubated for 20 min at ambient conditions. (b) Calibration curve used for calculation of N_2H_4 concentrations.

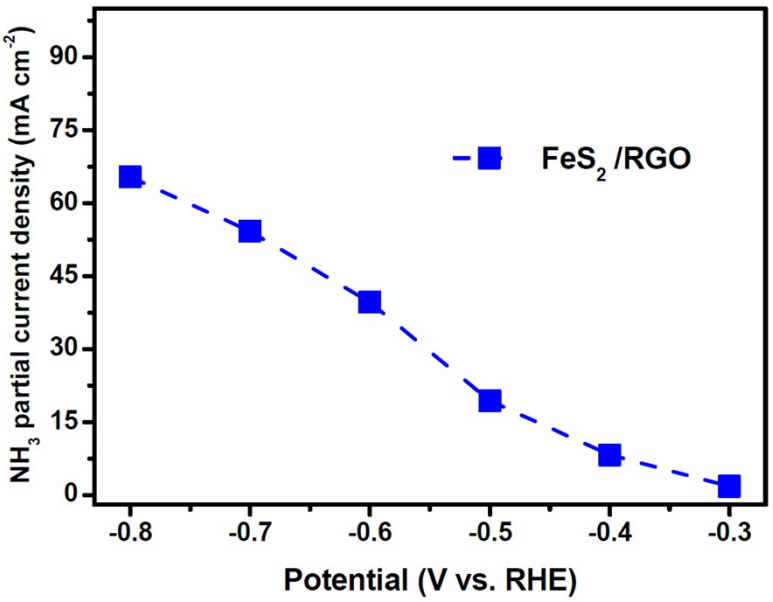

Fig. S6. NH_3 partial current densities of FeS_2/RGO at various potentials.

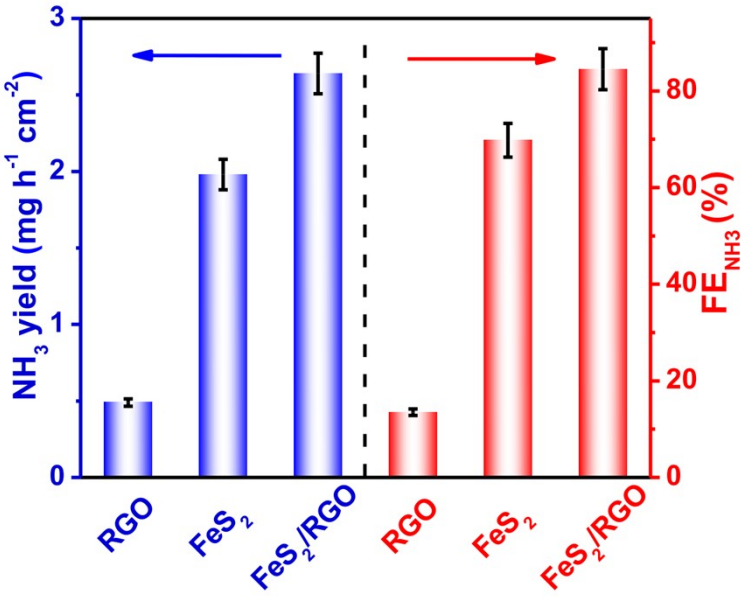

Fig. S7. NH_3 yields and FEs of RGO, FeS_2 and FeS_2/RGO at the optimal potential.

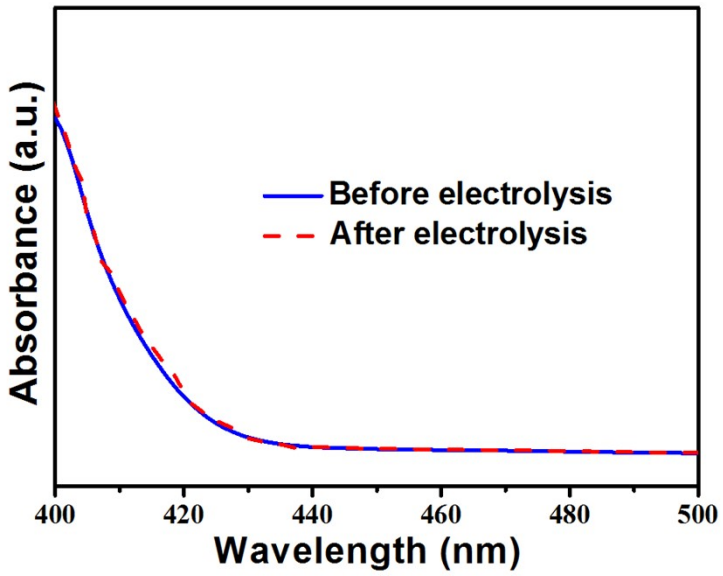

Fig. S8. UV-vis spectra of the electrolytes (stained with the chemical indicator based on the method of Watt and Chrisp) before and after electrocatalysis on FeS_2/RGO at -0.6 V.

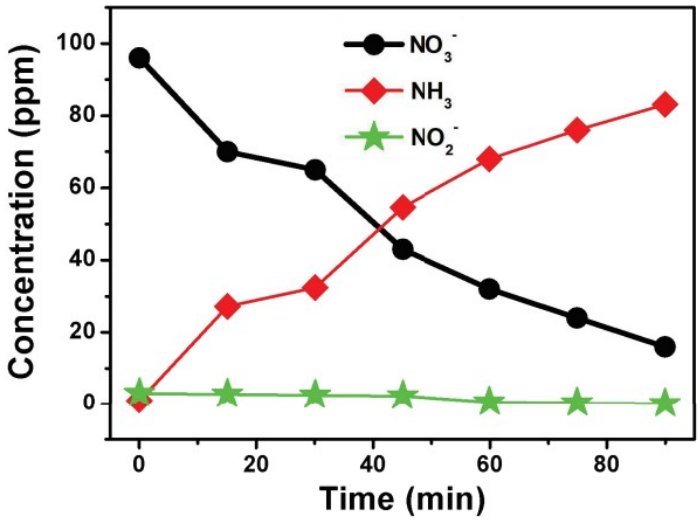

Fig. S9. Concentrations of NO_3^-, NH_3 and NO_2^- in the electrolyte at different electrolysis times at -0.6 V.

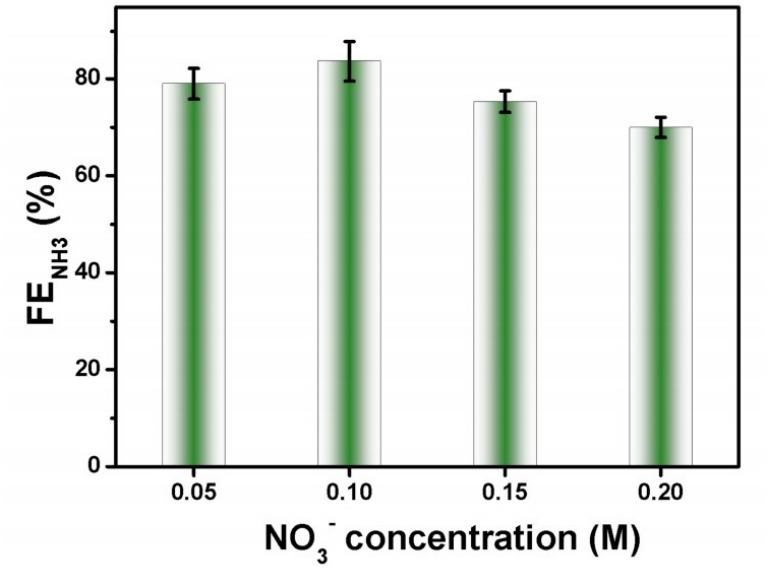

Fig. S10. FE_{NH3} at different NO_3^- concentrations.

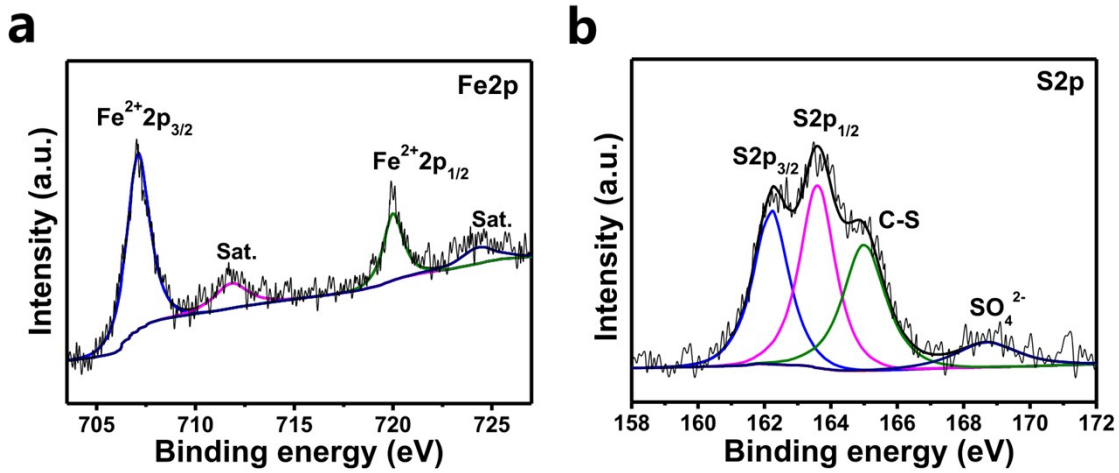

Fig. S11. XPS spectra of the FeS_2/RGO after stability tests: (a) Fe2p, (b) S2p

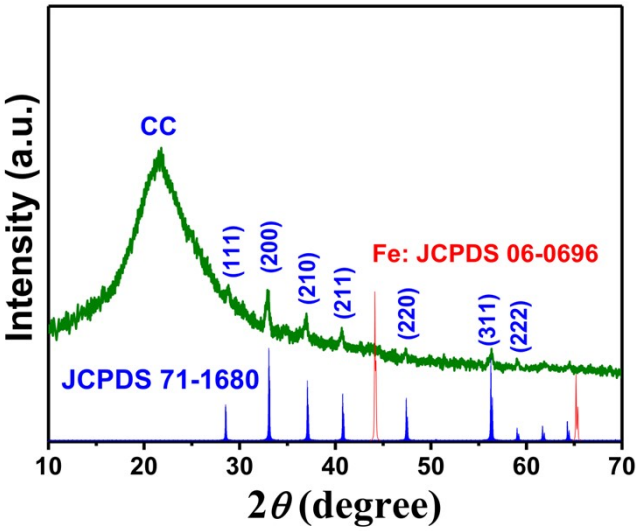

Fig. S12. XRD pattern of the FeS_2/RGO after stability tests.

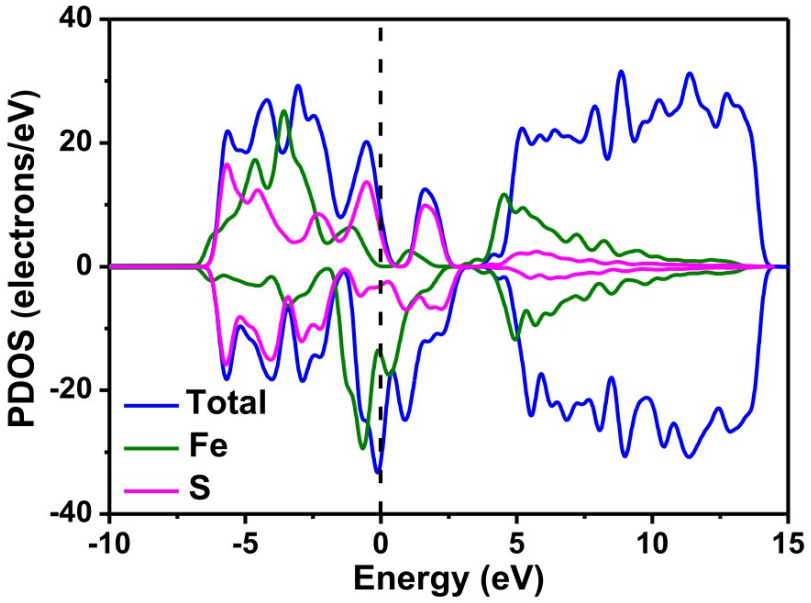

Fig. S13. PDOS of FeS_2 in both spin-up and spin-down states.

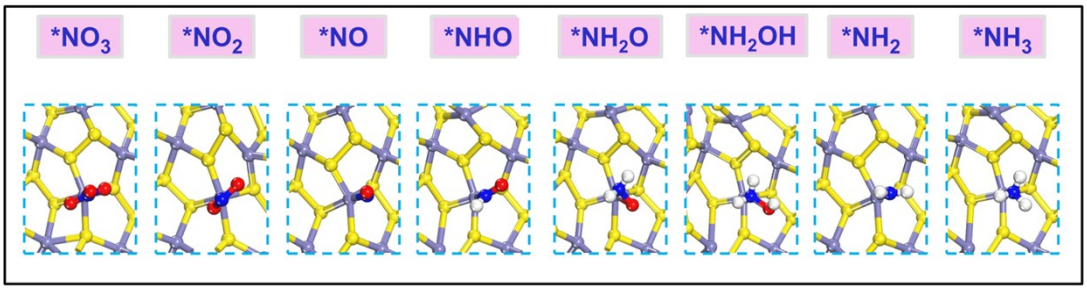

Fig. S14. Atomic structures of the reaction intermediates for NHO pathway on FeS_2.

Table S1. Comparison of the optimum NH_3 yield and Faradic efficiency (FE) for the recently reported NO_3RR electrocatalysts at ambient conditions.

Catalyst	Electrolyte	NH_3 yield rate	FE(%)	Potential (V vs RHE)	Ref.
CuCl_BEF	0.5 M Na_2SO_4 （100 mg/NO_3^-）	1.82 mg h^{-1} cm^{-2}	44.7	-1.0	13
dr-Cu NPs	0.5 M K_2SO_4 （50 ppm KNO_3）	0.78 mg h^{-1} mg_{cat}^{-1}	85.47	-1.3	14
RuNi-MOF	0.1 M Na_2SO_4 （50 mg L^{-1} NO_3^-）	0.27 mg h^{-1} mg_{cat}^{-1}	73	-1.2	15
Pd NDs/Zr-MOF	0.1 M Na_2SO_4 (500 ppm NO_3^-)	4.88 mg·h^{-1}·mg_{cat}^{-1}	58.1	-1.3	16
CoP/CC	1 M NaOH （2mM $NaNO_3$）	0.32 mg $h^{-1}cm^{-2}$	65	-0.4	17
10Cu/TiO_{2-x}	0.5 M Na_2SO_4 (200 ppm NO_3^-)	2.40 mg h^{-1} mg_{cat}^{-1}	81.34	-0.75	18
FC	0.05 M H_2SO_4 （200 ppm KNO_3）	0.40 mg h^{-1} mg_{cat}^{-1}	20	-0.65	19
Pd facets	0.1 M NaOH （20 mM NO_3^-)	0.31 mg $h^{-1}mg_{cat}^{-1}$	35	-0.2	20
Cu_2O	0.5 M Na_2SO_4 (200 ppm NO_3^-)	1.19 mg h^{-1} mg_{cat}^{-1}	85.26	-1.2	21
Cu−Pd/C	0.5 M H_2SO_4 0.1 M KOH	0.22 mg h^{-1} mg_{cat}^{-1}	62.3	-0.4	22
FeS_2/RGO	**0.5 M Na_2SO_4 （0.1 M NO_3^-）**	**2.32 mg h^{-1} cm^{-2} 4.64 mg h^{-1} mg_{cat}^{-1}**	**83.7**	**-0.6**	**This work**

Supplementary references

1. Y. Birdja, J. Yang and M. Koper, *Electrochim. Acta*, 2014, **140**, 518-524.
2. M. Ghazouani, H. Akrout and L. Bousselmi, *Environ. Sci. Pollut. Res.*, 2017, **24**, 9895-9906.
3. J. R. Christianson, D. Zhu, R. J. Hamers and J. Schmidt, *J. Phys. Chem. B*, 2014, **118**, 195-203.
4. J. Crawford, H. Yin, A. Du and A. P. O'Mullane, *Angew. Chem., Int. Ed.*, 2022, **134**, e202201604.
5. Y. Wang, H. Li, W. Zhou, X. Zhang, B. Zhang and Y. Yu, *Angew. Chem., Int. Ed.*, 2022, e202202604.
6. W. J. Sun, H. Q. Ji, L. X. Li, H. Y. Zhang, Z. K. Wang, J. H. He and J. M. Lu, *Angew. Chem., Int. Ed.*, 2021, **60**, 22933-22939.
7. P. Li, Z. Jin, Z. Fang and G. Yu, *Energy Environ. Sci.*, 2021, **14**, 3522-3531.
8. L. C. Green, D. A. Wagner, J. Glogowski, P. L. Skipper, J. S. Wishnok and S. R. Tannenbaum, *Anal. Biochem.*, 1982, **126**, 131-138.
9. X. Fan, L. Xie, J. Liang, Y. Ren, L. Zhang, L. Yue, T. Li, Y. Luo, N. Li, B. Tang, Y. Liu, S. Gao, A. A. Alshehri, Q. Liu, Q. Kong and X. Sun, *Nano Res.*, 2022, **15**, 3050-3055.
10. G. W. Watt and J. D. Chrisp, *Anal. Chem.*, 1952, **24**, 2006-2008.
11. Y. Wang, X. Qin and M. Shao, *J. Catal.*, 2021, **400**, 62-70.
12. P. Lv, D. Wu, B. He, X. Li, R. Zhu, G. Tang, Z. Lu, D. Ma and Y. Jia, *J. Mater. Chem. A*, 2022, **10**, 9707-9716.
13. W. J. Sun, H. Q. Ji, L. X. Li, H. Y. Zhang, Z. K. Wang, J. H. He and J. M. Lu, *Angew. Chem., Int. Ed.*, 2021, **60**, 22933-22939.
14. Y. Xu, M. Wang, K. Ren, T. Ren, M. Liu, Z. Wang, X. Li, L. Wang and H. Wang, *J. Mater. Chem. A*, 2021, **9**, 16411-16417.
15. J. Qin, K. Wu, L. Chen, X. Wang, Q. Zhao, B. Liu and Z. Ye, *J. Mater. Chem. A*, 2022, **10**, 3963-3969.
16. M. Jiang, J. Su, X. Song, P. Zhang, M. Zhu, L. Qin, Z. Tie, J.-L. Zuo and Z. Jin, *Nano Lett.*, 2022, **22**, 2529-2537.
17. H. Zhang, G. Wang, C. Wang, Y. Liu, Y. Yang, C. Wang, W. Jiang, L. Fu and J. Xu, *J. Electroanal. Chem.*, 2022, **910**, 116171.
18. X. Zhang, C. Wang, Y. Guo, B. Zhang, Y. Wang and Y. Yu, *J. Mater. Chem. A*, 2022, **10**, 6448-6453.
19. Y. Li, S. Xiao, X. Li, C. Chang, M. Xie, J. Xu and Z. Yang, *Mater. Today Phys.*, 2021, **19**, 100431.
20. J. Lim, C.-Y. Liu, J. Park, Y.-H. Liu, T. P. Senftle, S. W. Lee and M. C. Hatzell, *ACS Catal.*, 2021, **11**, 7568-7577.
21. Z. Gong, W. Zhong, Z. He, Q. Liu, H. Chen, D. Zhou, N. Zhang, X. Kang and Y. Chen, *Appl. Catal., B*, 2022, **305**, 121021.
22. Z. Wang, C. Sun, X. Bai, Z. Wang, X. Yu, X. Tong, Z. Wang, H. Zhang, H. Pang, L. Zhou, W. Wu, Y. Liang, A. Khosla and Z. Zhao, *ACS Appl. Mater. Interfaces*, 2022, **14**, 30969-30978.